# **Experimental Investigation of Thermal and Hydraulic Properties of Ice-Rich Saline Permafrost in Northern Alaska**

Ziyi Wang<sup>1</sup>; Ming Xiao<sup>2</sup>; Matthew Bray<sup>3</sup>; and Margaret Darrow<sup>4</sup>

<sup>1</sup>Dept. of Civil and Environmental Engineering, Pennsylvania State Univ., University Park, PA. Email: ziyiwang@psu.edu

<sup>2</sup>Dept. of Civil and Environmental Engineering, Pennsylvania State Univ., University Park, PA. Email: mzx102@psu.edu

<sup>3</sup>Institute of Northern Engineering, Univ. of Alaska Fairbanks, Fairbanks, AK.

Email: mtbray@alaska.edu

<sup>4</sup>Dept. of Civil, Geological, and Environmental Engineering, Univ. of Alaska Fairbanks, Fairbanks, AK. Email: mmdarrow@alaska.edu

## **ABSTRACT**

Unfrozen water content and thermal properties are factors in understanding permafrost degradation processes, yet there is a general lack of information on the hydro-thermal properties of relatively undisturbed ice-rich permafrost in Arctic coastal regions. In this research, we measured the unfrozen water content as a function of temperature in samples from near-surface undisturbed ice-rich permafrost using a pulsed nuclear magnetic resonance (P-NMR) testing system, in a temperature-controlled environment. We measured frozen and unfrozen thermal conductivity and heat capacity of the permafrost samples. The average frozen and unfrozen thermal conductivities are 2.23 and 1.30 W/m·K, respectively, and the average frozen and unfrozen heat capacities are 1.91 and 3.00 MJ/m³/K, respectively. To investigate the effect of salinity on unfrozen water content of permafrost, we measured the samples' salinity levels. The salinity levels of the permafrost samples varied, ranging from 0.5 to 15.2 parts per thousand. Based on these data, we established an empirical relationship between salinity and unfrozen water content for ice-rich organic silty permafrost that can be used for engineering purposes.

**Keywords:** permafrost, unfrozen water content, thermal properties, salinity, Alaska coasts

## INTRODUCTION

The Arctic is on the front line of global climate change and is warming up to four times faster than the rest of the planet (Rantanen et al. 2022). With rising air temperatures, ground temperatures elevate in the Arctic, leading to degradation of near-surface permafrost (Biskaborn et al., 2019). Various modes of permafrost degradation, including ground subsidence, active layer thickening, and talik formation, have already induced irreversible damages to Arctic civil infrastructure, threatening Indigenous Arctic communities and pan-Arctic economy (Andersland & Ladanyi 2003; Melvin et al. 2017; Hjort et al. 2018; Wang et al. 2023a, b).

Unfrozen water content and thermal properties are factors in permafrost degradation processes such as mass and heat transfer and thaw settlement. Understanding these properties is essential in analyzing and predicting the thermal-hydro-mechanical responses of degrading permafrost. Critical to this understanding is the correlation between temperature and unfrozen

water content of permafrost. Furthermore, thermal properties, including thermal conductivity and heat capacity in both frozen and unfrozen states, are essential for determining heat flux within permafrost environments.

Saline permafrost exists in the Arctic subsea and coastal zones, where marine deposits and seawater intrusions contribute significantly to the presence of dissolved salts (Osterkamp 1989; Brouchkov 2002). The causes of freezing point depression of soil include capillary effect of small pores, absorption at mineral surfaces, and dissolved salts in the pore water. Saline permafrost differs from its non-saline counterpart primarily due to the freezing-point depression induced by the presence of dissolved salts. As a result, saline permafrost typically remains partially thawed and exhibits mechanical weakness due to the reduced ice content available for sediment grain adhesion (Dou et al. 2016). Mechanical weakness may lead to increased vulnerability of infrastructure established on such ground, elevating risks of structural failure.

In this study, we conducted laboratory measurements and analysis of thermal properties of relatively undisturbed, ice-rich, saline silty permafrost. To measure the unfrozen water content of permafrost cores, we used a pulsed nuclear magnetic resonance (P-NMR) testing system within a temperature-controlled environment. We used power-law fitting to establish a volumetric unfrozen water content model with two parameters. We also carried out measurements on selected permafrost core samples to study the effect of salinity on the two unfrozen water content fitting parameters. Lastly, we provided an empirical equation to calculate the unfrozen water content of ice-rich, organic, silty permafrost with different salinity levels.

# FIELD SAMPLING AND PERMAFRSOT CHARACTERIZATION

In summer 2022, we sampled the upper 1.5 m of permafrost from five locations in the tundra near Utqiagvik, Alaska (Figure 1a). A battery-powered auger was used to extract relatively undisturbed permafrost samples (Figure 1b). As depicted in Figure 1c, the permafrost samples predominantly consisted of organic ice-rich silty soil. We retrieved a total of 562.1 cm of permafrost core, with a diameter ranging from 4.0 to 4.3 cm. Comprehensive analysis of the samples was conducted by the University of Alaska Fairbanks (UAF) Frozen Soil Testing (FROST) Laboratory. The tests included evaluations of thermal conductivity, heat capacity, unfrozen water content, and various mechanical properties. In this paper, we outline the testing methods and provide a summary of the results of thermal properties and unfrozen water content of the permafrost samples.

Figure 2 depicts the patterns of ice inclusions in the near-surface permafrost samples. The samples were exposed to a light source and the transparent ice layers are white or a light color. Ice layers are evident in cores S2-1, S2-2, S3-2, S5-4, S5-5, S5-6, and S5-7, with suspended thin organic bands generally less than 2-mm thick.

Figure 3 illustrates the permafrost specimens from sampling sites S2, S3, S4, and S5, showing notable stratigraphic variations. In the upper soil layers (*e.g.*, S2-1 and S4-1), the permafrost cores are primarily peaty with thin ice lenses or no visible ice. A marked increase in ice content was observed with greater depth across all sampling locations. These deeper soils were suspended in ice (ataxitic cryostructure), predominantly characterized as ice-rich silty sand intermixed with organic materials.



Figure 1. Field sampling of near-surface (upper 1.5 m) permafrost in the tundra near Utqiagvik, Alaska: (a) aerial views the five sampling locations (base map data from imagery copyright 2022 Maxar); (b) using battery-powered auger for permafrost sampling; and (c) relatively undisturbed permafrost.

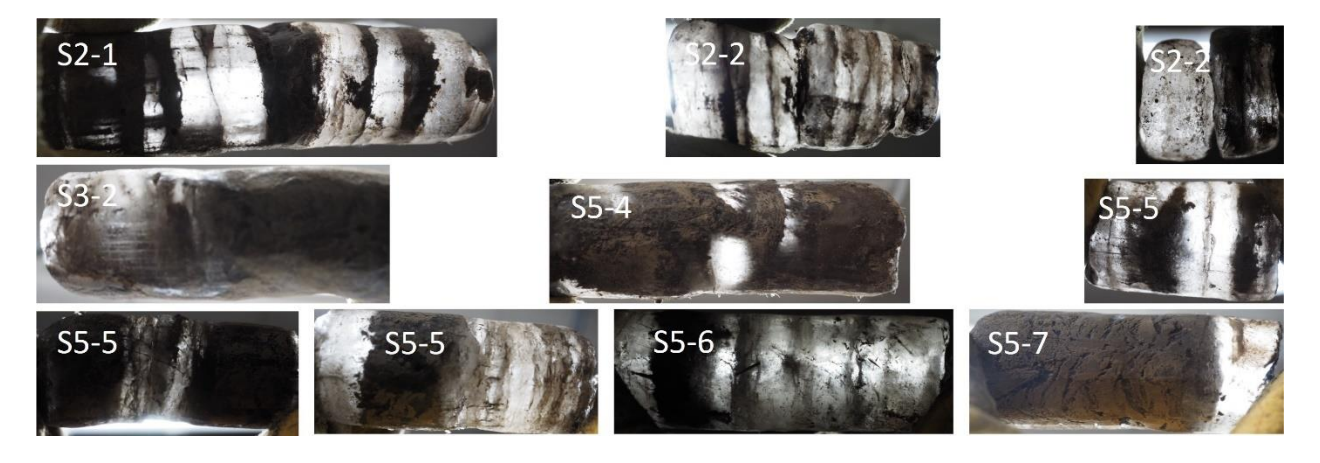


Figure 2. Patterns of ice inclusions in near-surface permafrost near Utqiagvik, Alaska. The samples were exposed to a light source and the transparent ice layers are white or a light color.



Figure 3. Photographs of permafrost specimens from sampling locations S2, S3, S4, and S5.

## LABORATORY TESTING

We tested 12 samples for frozen and unfrozen thermal conductivity, and frozen and unfrozen heat capacity using a Tempos Thermal Properties Analyzer with an SH-3 dual-needle probe. We prepared the samples by first trimming the frozen cores into small cylinders, then drilling 2-mm diameter holes into one of the cut ends. We inserted Arctic Silver thermal compound into the holes to establish complete thermal contact. The measurement probe was firmly inserted into the holes. We then placed the sample in a freezer at an average temperature of -18.6°C to reach thermal equilibrium. We made three to five thermal conductivity and heat capacity measurements for each frozen sample and allowed time for thermal equilibrium between each set of measurements. Once the tests were completed, the samples were allowed to thaw overnight in a sealed container. Then, we mixed each sample and reinserted the probe. The sample and the probe were sealed and placed in an insulated box. We made three to five thermal conductivity and heat capacity measurements for the unfrozen samples at an average room temperature of 22.1°C.

We measured 12 samples for variation of unfrozen water content with temperature using the P-NMR method. We generally followed the testing procedure summarized by Kruse et al. (2018). The P-NMR testing system includes using a modified refrigerator for the testing environment, an insulated box to maintain the operating temperature of the magnet, and a variable temperature probe, which precisely controls the sample temperature. We prepared the samples for unfrozen water content measurements by coring the larger core samples with a 1.4 cm hole saw, typically to a length of 4 cm. We measured the unfrozen water content at -20, -10,

-5, -3, -2, -1, -0.5, 5, and 10°C. After each change in temperature, samples were allowed to reach thermal equilibrium for 2 hours. The testing method has an accuracy of  $\pm$  2% gravimetric water content.

The salinity of the permafrost was determined by measuring the concentration of soluble salts in the soil. The test method follows the standard ISO 11265:1994 (ISO 1994). We used a Milwaukee MW802 Pro Combo Meter for salinity measurements (Figure 4). The samples were first thawed. We then prepared a soil-water suspension by mixing 50 g of dry, thawed samples and 250 mL of distilled water. The suspension was soaked for an hour to let the salt dissolve completely. We calibrated the instrument with a standard solution of 1413  $\mu$ S/cm. We rinsed the measuring probe with distilled water before taking each measurement in the suspension. We performed three salinity measurements for each sample. The conductivity meter measurements were converted to parts per thousand (ppt), which is approximately equivalent to g/L.

When the mass of total dry soil,  $m_t$ , and gravimetric water content, w, are known, the mass of pore water,  $m_w$ , in the permafrost cores can be determined. The salinity of the suspension,  $S_I$ , is the salinity of the soil-water mixture with 50 g of dry soil and 250 mL of distilled water. The soil-water mixture has a water content of 5 (or 500%). We assume the soluble salts are uniformly distributed in the pore water. The salinity of the pore water of the permafrost cores,  $S_2$ , is given by Eq. 1:

$$S_2 = \frac{m_{salt}}{m_w} = \frac{5S_1}{w} \tag{1}$$



Figure 4. The conductive meter used to measure the salinity in the soil and a beaker with soil-water suspension.

#### RESULTS

Table 1 is a summary of the thermal conductivity and heat capacity results. The average frozen and unfrozen thermal conductivities are 2.23 and 1.30 W/m·K, respectively, and the average frozen and unfrozen heat capacities are 1.91 and 3.00 MJ/m³/K, respectively. Table 2 summarizes the results of gravimetric unfrozen water content of the tested samples as a function of temperature ranging from -20°C to 10°C.

Table 1. Thermal conductivity, heat capacity, and total gravimetric water content of tested samples.

Sample	Depth		l conductivity V/m·K)		t capacity J/m³/K)	Total gravimetric water content (%)		
No.	(cm)	Frozen	Unfrozen	Frozen	Unfrozen	water content (%)		
S2-5	129.5 - 137.2	2.339	1.602	2.544	3.392	45.1		
S3-3	72.4 - 81.3	1.915	1.456	1.552	2.671	80.4		
S3-5	100.3 - 105.4	2.653	1.406	1.802	2.671	56.1		
S3-5	105.4 - 113.0	2.450	1.303	2.108	3.045	79.1		
S3-6	123.2 - 129.5	2.008	1.372	1.365	2.658	129.7		
S3-7	130.8 - 134.6	2.156	1.416	1.885	2.684	143.6		
S4-2	52.1 - 61.0	1.895	0.701	1.782	3.906	171.5		
S4-3	73.7 - 81.3	2.389	1.336	2.383	2.754	98.4		
S4-4	109.2 - 115.6	2.473	2.222	1.931	3.983	115.9		
S4-5	114.3 - 120.7	2.328	0.657	1.441	1.713	104.5		
S4-6	157.5 - 163.3	2.389	1.383	2.118	2.422	19.1		
S5-3	74.9 - 80.0	1.776	0.727	2.020	4.109	243.1		

Table 2. Unfrozen water content (gravimetric) of the tested samples at different temperatures.

Temperature (°C)	S2-4	S2-5	S3-3	S3-5	S3-6	S3-7	S4-2	S4-3	S4-3	S4-5	S4-6	S5-3
-20.02	4.3	3.3	3.1	2.1	2.0	2.3	5.4	1.3	1.4	1.6	1.5	12.1
-10.02	6.1	5.8	3.9	2.6	2.5	3.6	5.9	2.4	1.3	3.1	2.4	12.1
-5.01	9.2	9.3	5.4	3.7	4.1	6.7	8.1	3.2	3.0	6.5	3.8	14.6
-3.03	13.6	13.4	5.9	4.8	5.2	8.4	8.5	4.2	4.2	7.9	5.3	19.3
-2.01	18.3	19.3	6.9	5.7	6.7	11.1	9.5	5.1	4	10.9	7.3	19.9
-1.05	35	37.9	9.1	9.5	11.9	17.3	11.9	6.6	6.5	14.6	13.8	24.9
-0.54	54.8	53.8	13.1	14.2	18.2	25.4	15	9.9	11	20.4	19.9	27.7
+4.79	76.4	81.2	65.2	53.8	67	114.2	186.9	82.7	80.9	148.2	26.2	537.5
+9.98	75.1	80.9	66.7	51.8	67.9	105.7	185.6	83.3	83.6	147.1	26.1	525.7

Figure 5 contains the experimental results of normalized volumetric unfrozen water content of all samples as a function of temperature for the sub-freezing temperatures. The volumetric unfrozen water content,  $\theta_u$ , is normalized by total volumetric water content,  $\theta$ , to have a range between 0 to 1. The relationship between the normalized volumetric unfrozen water content,  $\theta_{n,u}$ , and temperature, T, can be presented in the form of a simple power law (Anderson and Tice 1973; Bray 2013):

$$\theta_{n,u} = C \left(\frac{T}{T_0}\right)^b \tag{2}$$

where  $T_0$  is the reference temperature of -1°C, and C and b are two parameters determined by curve-fitting (Figure 5).

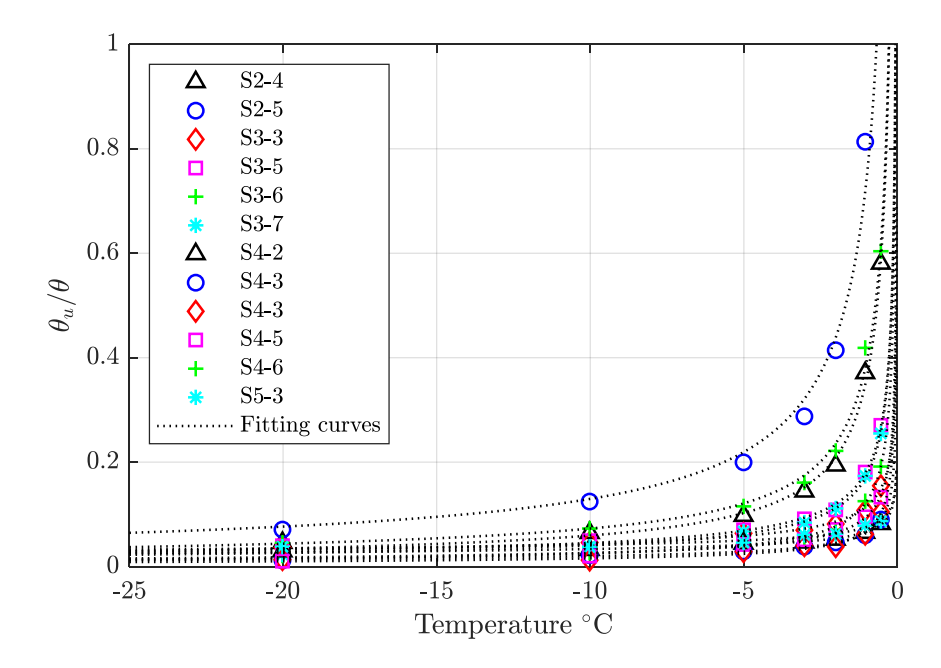


Figure 5. Experimental results of normalized volumetric unfrozen water content  $(\theta_u/\theta)$ . The black dashed lines are fitting curves.

Table 3 details the index properties, the salinity, and parameters of the power law model, b and C, of the 12 selected permafrost samples subjected to unfrozen water content analysis. Power law models exhibit a robust correlation with the experimental data, evidenced by  $R^2$  values ranging between 0.969 to 0.998.

Table 3. Index properties, parameters of the power law model for unfrozen water content, and salinity of the tested samples.  $\rho_{bf}$  is the bulk frozen density,  $\rho_{dry}$  is the dry density, w is the gravimetric water content, and C, b are the parameters of the power law model of unfrozen water content.

Sample No.	Depth	$ ho_{bf}$	$ ho_{dry}$	W	Salinity	C	b	$R^2$
Sample No.	(cm)	(g/cm <sup>3</sup> )	(g/cm <sup>3</sup> )	(%)	(ppt)		D	
S2-4	105-113	1.38	0.73	89.1	9.42	0.3619	-0.7835	0.996
S2-5	130-137	1.22	0.84	45.1	15.24	0.7452	-0.7594	0.987
S3-3	135-141	1.28	0.71	80.4	2.16	0.1156	-0.4187	0.986
S3-5	92-100	1.57	1.05	50.1	5.45	0.1842	-0.6102	0.993
S3-6	114 - 122	1.38	0.73	89.5	4.10	0.1250	-0.6953	0.995
S3-7	146 - 155	1.37	0.71	93.8	3.79	0.1741	-0.6335	0.998
S4-2	52-61	1.16	0.43	171.5	0.84	0.0667	-0.2980	0.987
S4-3	65-74	1.32	0.65	103.3	1.36	0.0649	-0.5081	0.994
S4-3	74-81	1.39	0.70	98.4	2.22	0.0688	-0.6403	0.977
S4-5	132-141	1.35	0.67	102.9	5.36	0.0961	-0.5627	0.986
S4-6	147 - 156	1.82	1.38	31.7	8.03	0.3934	-0.7320	0.991
S5-3	64-72	1.05	0.27	295.9	0.46	0.0760	-0.2603	0.969

#### ANALYSIS AND DISCUSSIONS

Figure 6 is a plot of the salinity conditions with the two parameters, C and b, of the power law model of unfrozen water content. We used a logarithmic best-fit line to describe the relationship between parameter b and salinity (Figure 6a). We applied a linear best-fit line to correlate parameter C with salinity (Figure 6b). Both logarithmic and linear fittings demonstrate a strong correction with  $R^2$  values of 0.828 and 0.912, respectively. For predictive purposes, parameters b and C can be estimated from Eq. 3 and 4:

$$b = -0.153 \ln x - 0.3958 \tag{3}$$

$$C = 0.0451x - 0.0138 \tag{4}$$

where x is salinity level in ppt. It is worth noting that the unfrozen water content may vary significantly depending on the cryostructure, soil type, and ice content. The correlation model discussed above was developed based on ice-rich organic silty permafrost with ataxitic cryostructure obtained in the tundra near Utqiagʻvik, Alaska.

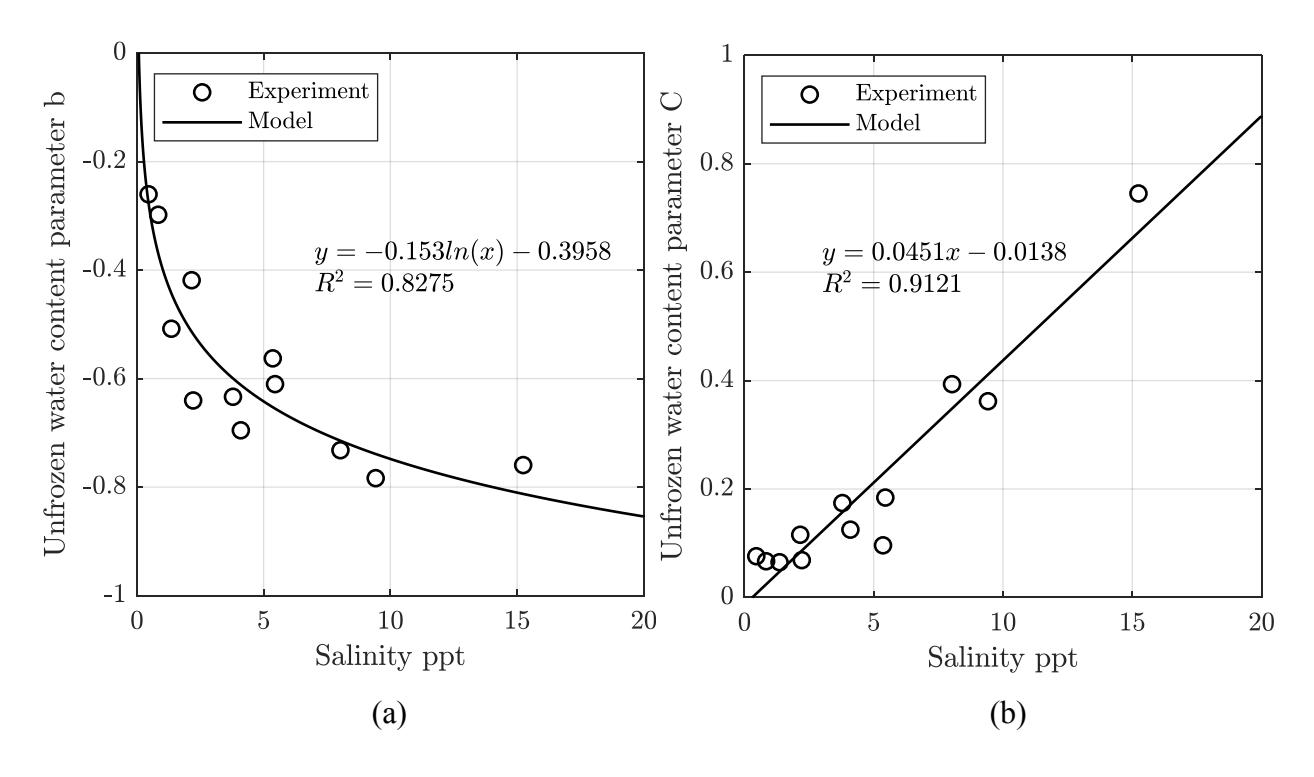


Figure 6. Relationships between parameters of unfrozen water content and salinity: (a) best fitting model for parameter b with salinity level; and (b) best fitting model for parameter C with salinity level.

Figure 7 is a plot of the correlation model for ice-rich organic silty permafrost for engineering purposes. The chart relates the normalized unfrozen water content to temperature and salinity. As per Eq. 2, 3, and 4, the normalized unfrozen water content increases with increasing temperature and salinity in the pore water.

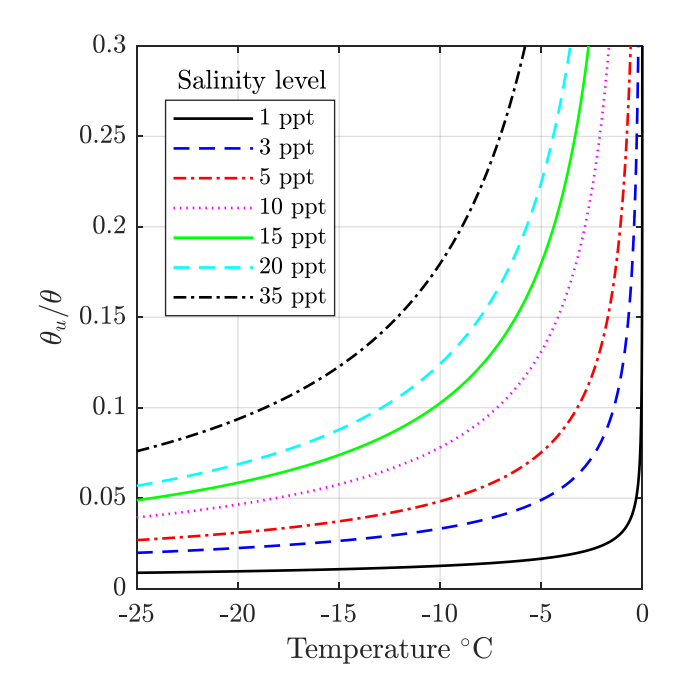


Figure 7. Variation of normalized unfrozen water content with salinity levels and temperature for ice-rich silty permafrost.

## CONCLUSIONS

In this study, we conducted experimental investigations on the thermal properties and unfrozen water content of near-surface (upper 1.5 m) saline permafrost in the tundra near Utqiagvik, Alaska. The permafrost soils are primarily organic and ice-rich with ataxitic cryostructure (i.e., soil suspended in ice). We measured the thermal conductivity and heat capacity of 12 permafrost samples. The average frozen and unfrozen thermal conductivities are 2.23 and 1.30 W/m·K, respectively, and the average frozen and unfrozen heat capacities are 1.91 and 3.00 MJ/m³/K, respectively. We analyzed the unfrozen water content of 12 permafrost samples as a function of temperature. The salinity levels of the permafrost samples varied, ranging from 0.5 to 15.2 parts per thousand. To understand the effect of salinity on unfrozen water content, we evaluated the salinity in each sample and proposed an empirical model that correlates salinity with unfrozen water content in ice-rich organic silty permafrost.

# **ACKNOWLEDGEMENTS**

This study was supported by the U.S. National Science Foundation under Grant Numbers: ICER-1927718 and CMMI- 2034363.

# REFERENCES

Andersland, O.B. and Ladanyi, B., 2003. *Frozen ground engineering*. John Wiley & Sons. Anderson, D.M. and Tice, A.R., 1973. The unfrozen interfacial phase in frozen soil water systems. In *Physical aspects of soil water and salts in ecosystems* (pp. 107-124). Berlin, Heidelberg: Springer Berlin Heidelberg.

- Biskaborn, B.K., Smith, S.L., Noetzli, J., Matthes, H., Vieira, G., Streletskiy, D.A., Schoeneich, P., Romanovsky, V.E., Lewkowicz, A.G., Abramov, A. and Allard, M., 2019. Permafrost is warming at a global scale. *Nature communications*, 10(1), p.264.
- Bray, M.T., 2013. Secondary creep approximations of ice-rich soils and ice using transient relaxation tests. *Cold regions science and technology*, 88, pp.17-36.
- Brouchkov, A., 2002. Nature and distribution of frozen saline sediments on the Russian Arctic coast. *Permafrost and Periglacial Processes*, 13(2), pp.83-90.
- Dou, S., Nakagawa, S., Dreger, D. and Ajo-Franklin, J., 2016. A rock-physics investigation of unconsolidated saline permafrost: P-wave properties from laboratory ultrasonic measurements. *Geophysics*, 81(1), pp. WA233-WA245.
- Hjort, J., Karjalainen, O., Aalto, J., Westermann, S., Romanovsky, V.E., Nelson, F.E., Etzelmüller, B. and Luoto, M., 2018. Degrading permafrost puts Arctic infrastructure at risk by mid-century. *Nature communications*, 9(1), p.5147.
- ISO, 1994. Soil Quality. Determination of the Specific Electrical Conductivity.
- Kruse, A.M., Darrow, M.M. and Akagawa, S., 2018. Improvements in measuring unfrozen water in frozen soils using the pulsed nuclear magnetic resonance method. *Journal of Cold Regions Engineering*, 32(1), p.04017016.
- Melvin, A.M., Larsen, P., Boehlert, B., Neumann, J.E., Chinowsky, P., Espinet, X., Martinich, J., Baumann, M.S., Rennels, L., Bothner, A. and Nicolsky, D.J., 2017. Climate change damages to Alaska public infrastructure and the economics of proactive adaptation. *Proceedings of the National Academy of Sciences*, 114(2), pp.E122-E131.
- Osterkamp, T.E., 1989. Occurrence and potential importance of saline permafrost in Alaska: Workshop on Saline Permafrost. University of Manitoba.
- Rantanen, M., Karpechko, A.Y., Lipponen, A., Nordling, K., Hyvärinen, O., Ruosteenoja, K., Vihma, T. and Laaksonen, A., 2022. The Arctic has warmed nearly four times faster than the globe since 1979. *Communications Earth & Environment*, 3(1), p.168.
- Wang, Z., Xiao, M., Liew, M., Jensen, A., Farquharson, L., Romanovsky, V., Nicolsky, D., McComb, C., Jones, B.M., Zhang, X. and Alessa, L., 2023a. Arctic geohazard mapping tools for civil infrastructure planning: a systematic review. *Cold Regions Science and Technology*, p.103969.
- Wang, Z., Xiao, M., Nicolsky, D., Romanovsky, V., McComb, C. and Farquharson, L., 2023b. Arctic coastal hazard assessment considering permafrost thaw subsidence, coastal erosion, and flooding. *Environmental Research Letters*, 18(10), p.104003.